Stochastic Reactor-Based Fuel Bed Model for Grate Furnaces

Corinna Netzer,[*,†] Tian Li,[†,‡] Lars Seidel,[¶] Fabian Mauß,[§] and Terese Løvås[†]

†*Department of Energy and Process Engineering, Norwegian University of Science and Technology, Trondheim, Norway*

‡*RISE Fire Research, Tiller, Norway*

¶*LOGE Deutschland GmbH, Cottbus, Germany*

§*Chair of Thermodynamics and Thermal Process Engineering, Brandenburg University of Technology, Cottbus, Germany*

E-mail: corinna.netzer@ntnu.no

Abstract

Biomass devolatilization and incineration in grate fired plants are characterized by heterogeneous fuel mixtures, often incompletely mixed, dynamical processes in the fuel bed and on particle scale, as well as heterogeneous and homogeneous chemistry. This makes modelling using detailed kinetics favorable, but computationally expensive. Therefore a computational efficient model based on zero-dimensional stochastic reactors and reduced chemistry schemes, consisting of 83 gas phase species and 18 species for surface reactions, is developed. Each reactor is enabled to account for the three phases; the solid phase, pore gas surrounding the solid and bulk gas. The stochastic reactors are connected to build a reactor network that represents the fuel bed in grate fired furnaces. The use of stochastic reactors allows to account for incompletely mixed fuel feeds and distributions of local temperature, local equivalence ratio within each reactor and the fuel bed. This allows to predict the released gases and emission precursors

more accurately than if a homogeneous reactor network approach was employed. The model approach is demonstrated by predicting pyrolysis conditions and two fuel beds of grate fired plants from literature. The developed approach can predict global operating parameters such as the fuel bed length and species release to the freeboard as well as species distributions within the fuel bed to a high degree of accuracy when compared to experiments.

Nomenclature

β	Porosity source factor	-
β_m	Mixing constant	-
$c_{p,g}$	Gas phase specific heat capacity at constant pressure	J /(kgK)
C_ϕ	Mixing time constant	-
D	Mass diffusivity	m^2/s
d_s	Solid particle's representative diameter	m
ϵ	Porosity	-
ε_p	Emissivity of the solid particle	-
ε_w	Emissivity of the wall	-
F_Φ	Mass density function	-
λ	Heat conductivity	W/(mK)
μ_g	Dynamic viscosity	m^2/s
m_s	Solid species' mass	kg
n_s	Number of solid particles	-
Nu_p	Particle's Nusselt number	-
Φ	Random variable	unit depending on variable
φ	Fuel air equivalence ratio	-
ψ	Realization of any random variable	unit depending on variable
P_2	Mixing term	-
Pr	Prandtl number	-
q_{rad}	Radiation term	$J/(m^2s)$
Q_i	Source term function	-
ρ_g	Density gas phase	kg/m^3
ρ_s	Solid density	kg/m^3
Re_p	Particle's Reynolds number	-
σ	Stefan-Boltzmann constant	$W/(m^2K^4)$
S	Number of species in the reaction mechanism	-
Sc	Schmidt number	-
Sh	Sherwood number	-
τ	Residence time	s
τ_{mix}	Scalar mixing time	s
t	Time step	s
T_s	Solid's temperature	K
T_w	Wall temperature	K
$V_{s,tot}$	Total volume of all solid particles	m^3
v_{slip}	Slip velocity	m/s
$\omega_{i,s}$	Sources term chemistry integration of species i from solid reactions	$kg/(m^2s)$

Introduction

The combustion of biomass has the potential to offer the generation of renewable energy and heat supply from local available resources. The burned biomass is often waste material from wood, forest and food industry and utilised locally for in-house energy supply. These fuels can vary in size, composition and water content. Moving grate firing systems are widely applied to burn biomass since they have a simple construction and process control. In addition, they offer the needed flexibility towards the varying fuel and have low investment costs.[1] However, the drawback of this diverse use of the technology, is unoptimized incineration that leads to unwanted levels of emissions such as dust and nitrogen oxides (NO_x) as well as incomplete combustion products, such as carbon monoxide (CO), unburned hydrocarbons (HC) and poly-cyclic aromatic hydrocarbons (PAHs) that can grow to soot particles.[2,3]

In order to optimize the combustion chamber design and operating modes, so to reduce primary emission formation as well as maximise the efficiency, the physical and chemical processes in the fuel bed on the grate needs to be better controlled. Insights can been gained by experimental studies both on lab scale[4,5] and in industrial plants,[6,7] as well as by the use of numerical simulations.[8–13]

In numerical simulations, the incineration of solid particles, within a multi-phase framework including heterogeneous and gas phase chemistry and different scales in time and space, poses challenges regarding the mathematical description of the problem. At the largest scale, the single particles and the interstitial gas phase involving turbulent flow and particle-particle interactions have still to be accounted for. At the single-particle level, heterogeneous reactions between the particle surface and the surrounding gas phase occur, and those reactions have to be described as functions of the varying fuel, composition of the released gases and local thermodynamic conditions. To resolve the chemical progress, ideally heat transfer between the particles, radiation from the freeboard, and mass transport of oxidizers towards the particle and product gases away from it, have to be depicted. At the molecular level, primary pyrolysis reactions and secondary tar and char cracking reactions should also be

considered. This multi-scale problem becomes exceptionally challenging when describing grate furnace devices of large dimensions with a high number of solid particles.

The *chemical processes* involved can be described by more or less detailed reaction schemes. Those schemes incorporate sub-processes such as the biomass devolatilization, which describes the biomass degradation into permanent gases, tars and char; the heterogeneous reactions on the solid surface between solid and gas phase; the secondary gas phase reactions of char and tar;[14] the oxidation of the released gases in the freeboard combustion and emission pathways. Examples for such schemes have been reported in previous studies.[14–17] Advantages of the most detailed schemes are outlined as follows.[18] (1) Any biomass can be modeled by a set of representative components based on either measured H:C:O-ratio or literature data. In previous studies biomass was e.g. represented by cellulose (CELL), hemicellulose (HCE) and lignin (LIG)[15,16,19] and extended by hydrophobic and hydrophilic extractives to enlarge the represented H:C:O-space.[20,21] (2) For each of those components decomposition path ways are described using a set of semi-detailed reactions rather than assumed global steps.[18] Such semi-detailed schemes predict correctly the mass loss evolution[18] to conserve mass in the chemical integration step during modelling. (3) Released gases are described by a detailed reaction scheme with contributions from different species classes which are: permanent gases, carbonyls, alcohols, monomeric phenolics, sugars, heterocyclics and water vapour. The gas reactions are described with detailed pathways without the introduction of lumped species or further assumptions.[18] (4) Char formation and conversion can further be described using heterogeneous reactions with the surrounding gas phase.[18] (5) The species pool and emission precursors that are needed to predict combustion and emissions in the freeboard of grated fired plants are finally incorporated.

Computational fluid dynamic (CFD) simulations offer the most comprehensive description of the the *physical processes* of particle decomposition, such as particle-particle inter-

actions or shrinking and the turbulent gas flow. Yet, the solid fuel bed and overbed gas (freeboard) combustion are often decoupled due to the high computational cost.[22] In literature, mainly three different ways to model the solid fuel bed have been proposed. The first model approach describes the fuel bed as a continuous porous medium, as applied e.g. by Collazo et al.[23] and Peters at al.[24] The second model approach is based on empirical correlations. Temperatures and species can be estimated using experimental databases or conversion rates.[25–27] Both of these model groups are computationally cheap and can be combined with freeboard models, but are not suitable for sensitivity analysis of fuel bed characteristics.[22] This sensitivity can only be provided by detailed models, in which usually the fuel bed and the freeboard are treated separately to limit computational cost. Detailed models can predict particle sizes, moisture content, solid particle density, effective thermal conductivity, specific heating value, primary air flow rate as well as the rate of heat and mass transfer.[22] They vary in their particle treatment; single particle models,[28–31] continuous media models[32–34] or particle resolved models.[35–37] Those complex physical models often use single Arrhenius type approximations for chemical reactions. The applied kinetic rates are applicable specially for the given type of biomass. Hence, lumped species, together with global step or skeletal gas phase reaction mechanisms, are typically used.[22] When employing detailed surrogate formulations and reaction mechanisms with more than 20 species, the computational cost for CFD simulations can therefore become unreasonably high for engineering and optimization purposes.

Reduced order modelling can overcome the computational cost limitations while using detailed chemistry and including the treatment of the particles and other physical processes. A common approach in chemical process engineering is the use reactor network models, also called compartmental models.[38] Those models build on the assumption that the combination of ideal zero-dimensional (0D) and one-dimensional (1D) reactors can represent a nonideal reactor.[39] The equivalent reactor network (ERN) model[40–42] is nowadays widely used and

has been proven to be able to predict multi-phase flows including pyrolysis and gasification processes in spouted bed gasifiers,[39] opposed multiburner gasifiers,[43] fluidized catalytic cracking units[44] and for emission prediction of gas/oil-fired furnaces.[45] To create such ERN models, the computational domain is dived into smaller zones based on the hydrodynamics of the multi-phase flow. Each of those zones are then represented by a suitable ideal reactor in steady state operation.[39] Originally, ERN models were applied for highly turbulent flows, which are not suitable for simulating a fixed bed with a low turbulence air flow crossing. Therefore, models have been proposed that consider the geometry and height of the fuel bed. In these approaches several reactors are stacked on top of each other to represent a certain slice of the fuel bed, and several of those slices are placed in a row to represent the grate length. This concept has been used to predict waste decomposition in a 1D experimental bed reactor[46] and for biomass conversion in grate fired plants.[16,19,47] Those approaches assume that horizontal temperature and species gradients are small enough to be neglected and that gas phase and solid are distributed homogeneously within the reactors. However, for optimization of plant efficiency and for emission prediction, even reduced order models should account for the fuel beds transient behavior and the temperature distribution within the fuel bed.[16,48,49]

Different to ideal reactors, stochastic reactor models (SRM)[50,51] solves for the joint probability density function of species mass fraction and temperature within the reactor. Therefore, SRM offers the treatment of inhomogenity in temperature and species distribution. The use of stochastic reactors is beneficial over homogeneous reactors when reactors have multiple inlets with different compositions or incomplete mixed inlets. Within SRM, inhomogeneity evolves due to stochastic mixing and stochastic treatment of the heat transfer. For solid fuel conversion, such a stochastic reactor concept was introduced and developed for pyrolysis and gasification processes in a drop tube reactor by Weber et a.[52] within the commercial LOGEsoft software suite[53] using a simplified plug flow reactor type approach.

To the authors knowledge, this is the first time a network approach using *stochastic* reactors to describe solid fuel incineration has been demonstrated. This approach combines the benefit of reduced order modelling; detailed chemistry that includes complex emission and precursors formation, as well as accounting for inhomogenity of the fuel streams. This gives consideration for incomplete mixing in the fuel bed, such as channel formation or hot spots without the explicit description of those phenomena. The model is targeted to predict the gas phase distribution released by the fuel bed, which can be used as input for CFD simulations, or be connected to stochastic reactors representing the freeboard of a biomass incineration plant to predict emissions.

The paper is organized as follows: after the introduction of the model concept, its applicability is demonstrated using three different test cases. In Case 1,[14] the model approach and a reduced chemistry are validated under pyrolysis conditions towards speciation. Case 2[7] predicts the gas release from the bed of a biomass incineration plant with traveling grate that is ignited via radiation from the top of the fuel bed. In a second step, the released gases are used as input for CFD simulations of different loads. Case 3[54] represents a challenging case of wet biomass incineration with more than 50% water content in the solid. It is validated against species and temperature measurements within the bed. In this case, the fuel bed is operated in another combustion mode than Case 2, namely that it is ignited close to the grate surface and has an upwards moving reaction front together with the air flow.[54–56]

The Fuel Bed Model

The Stochastic Reactor Model for Solid Fuel Conversion

In this work, a reactor network was built using the SRM for solid fuel conversion[52] with LOGEresearch 1.10.[53]

The SRM is built on the PDF approach for reactive flows and the partially stirred reactor assumption.[57,58] The reactor mass is discretized into virtual packages that are called

stochastic particles. The virtual packages represent a discrete realization of the joint PDF of species and enthalpy. The mixing of the particles and the chemistry integration in each particle governs the evolution of the PDF and hence the combustion processes. This allows to account for inhomogenity in species and temperature field, while a stochastic particle itself is assumed to be homogeneous, so that chemistry can be solved without further assumptions. Due to the reduced spatial order (0D) of a stochastic reactor, the flow field is not solved and stochastic particles have no spatial position or motion, hence transport equations are only solved for the joint PDF F_Φ:[53,57]

$$\begin{aligned} &\frac{\partial}{\partial t} F_\Phi(\psi, t) + \frac{\partial}{\partial \psi_i} \left[Q_i(\psi) F_\Phi(\psi, t) \right] \\ &+ \frac{1}{\tau} \left[F_{in} - F_\Phi(\psi, t) \right] = P_2 F_\Phi(\psi, t) \end{aligned} \tag{1}$$

where Φ is a vector of random variables ($\Phi_1, ...\Phi_{S+1}$, where S is the number of chemical species), ψ is its realization in their sample space $\psi_1, ...\psi_{S+1}$ and $Q_i(\psi)$ are source terms due to chemical reactions and heat transfer. The term including the residence time τ accounts for mass in- and outflow of the reactor. The term P_2 on the right hand side describes the mixing of the particles and must be closed by means of a mixing model. In this work, the Curl mixing model is applied:[59]

$$\begin{aligned} P_2 F_\Phi(\psi, t) &= \frac{C_\Phi \beta_m}{\tau_{mix}} \\ &\left[\int_{\Delta\psi} F_\Phi(\psi - \Delta\psi, t) F_\Phi(\psi + \Delta\psi, t) d(\Delta\psi) - F_\Phi(\psi, t) \right]. \end{aligned} \tag{2}$$

The mixing model includes the scalar mixing time τ_{mix} and two model constants, which are set to $\beta_m = 1$ and $C_\phi = 2$.[60]

There are two key parameters important for the SRM. (1) The mixing time, scalar, is a measure of how often the stochastic particles are mixed with each other within a time

step, and determines the homogeneity of the reactor. The smaller the mixing time, the more mixing events per time unit are performed, and the closer the stochastic reactor converges to a homogeneous reactor. (2) The number of stochastic particles is a measure of discretization. As for temporal or spacial discretization in CFD simulations, a very fine discretization, i.e. infinite number of particles, is ideal, while a too low number results in discretization errors.

In the SRM for solid fuel conversion, each stochastic particle contains three phases: the solid phase, pore gas surrounding the solid and bulk gas. Each of these phases have their own chemical composition and are assumed to be distributed homogeneously within a stochastic particle. For the full set of equations for species composition and temperature prediction the reader is referred to earlier studies.[52,53] For readability of this paper, some sub-models and assumptions are discussed in the following. The fuel conversion is calculated based on detailed chemistry schemes for heterogeneous reactions as well as oxidation of the released tar and gases. The chemistry integration is embedded in the operator splitting loop to solve the joint PDF (equation 1) in the following sequence:[53]

1. Inflow of mass
2. Mixing of the stochastic particles gas phase
3. Heterogeneous reactions and transport
4. Gas phase chemistry integration and radiation
5. Stochastic heat transfer
6. Outflow of mass

Note that only the gas phase of the stochastic particles are mixed, while solids and their surrounding bulk gases remain in their primary particle. The gas phase chemistry is solved as described in previous works[53,61] and the heterogeneous reactions are discussed elsewhere.[53,62] In the operator splitting loop, two processes are based on random seed generation: the selection of stochastic particles for mixing and the heat transfer with the wall. Both contribute to

keeping the inhomogeneity of an incomplete mixed inflow, but increase also inhomogenity by generating an inhomogeneous temperature field that leads to a different progress of reactions in each particle, that again gets mixed.

The solid particles are characterized by their porosity ϵ and representative diameter d_p. The mass of solids m_s is consumed by heterogeneous reactions. Therefore, the source terms from chemistry of each solid species $\omega_{i,s}$ are used to calculate reduction in solid mass:[53]

$$\frac{dm_s}{dt} = -V_{s,tot} \sum_{i=1}^{n_s} \omega_{i,s} \tag{3}$$

where $V_{s,tot}$ is the total volume of all solid particles in one stochastic particle. Based on the reduction of solid mass, the representative solid particle diameter is calculated using the solid density ρ_s and the number of solid particles n_s in each stochastic particle:[53]

$$\frac{dd_p}{dt} = \left(\frac{6}{\pi \rho_s n_s}\right)^{1/3} \frac{m_s^{-2/3}}{3} \frac{dm_s}{dt}. \tag{4}$$

The solid particle's porosity is updated using the chemical species source terms and a user-defined parameter for density evolution β:[53]

$$\frac{d\epsilon}{dt} = \frac{(1-\epsilon)(1-\beta)}{\rho_s} \sum_{i=1}^{n_s} \omega_{i,s}. \tag{5}$$

From these properties, the surface available for heterogeneous reactions and the solid concentration within the stochastic particle are calculated. The heterogeneous reactions occur between the solid phase and the pore gas. A local thermal equilibrium between the two phases is assumed. Gases are released into the pore gas and are then transported from pore to bulk gas. The model approach is schematically shown in Figure 1. Mass and heat transport coefficients are calculated using the Nusselt Nu and Sherwood Sh numbers, which are based on the particle's Reynolds number Re_p, the Prandtl number Pr and Schmidt numbers

Sc_S of the species S:[53]

$$Nu_p = 1.32 Re_p^{1/2} Pr^{1/3}, \tag{6}$$

$$Sh_S = 1.32 Re_p^{1/2} Sc_S^{1/3}, \tag{7}$$

$$Re_p = \frac{\rho_g |v_{slip}| d_p}{\mu_g}, \tag{8}$$

$$Pr = \frac{c_{p,g} \mu_g}{\lambda}. \tag{9}$$

$$Sc_S = \frac{\mu_g}{\rho_g D_S}. \tag{10}$$

In the reactor network, the term accounting for wall temperature (boundary temperature) is used to calculate the radiation from the freeboard onto the bed; or in case the bed is ignited from the bottom, to initialize a heat source to start reactions. Radiation from the reactor walls towards the solid particles is calculated by[53]

$$q_{rad} = \sigma \varepsilon_p \varepsilon_w (T_s^4 - T_w^4) \tag{11}$$

where σ is the Stefan-Boltzmann constant, ε_p and ε_w are the emissivity of the solid particle and the wall, and T_s and T_w the solid and wall temperature, respectively.

The Reactor Network Approach

For the reactor network, stochastic reactors are connected and mass flows with their respective species composition and temperatures are transferred between the reactors. The fuel transport over the grate and the mixing rate are input parameters. Therefore, the residence time and mixing intensity can be varied to account for different fuel bed types, such as fixed bed reactors, fixed grate, moving grate or rotary furnaces.

In the reactor network, every reactor can have as many inlet and outlet streams as wanted. However, here each reactor has maximum three in- and two out-flowing streams due to the

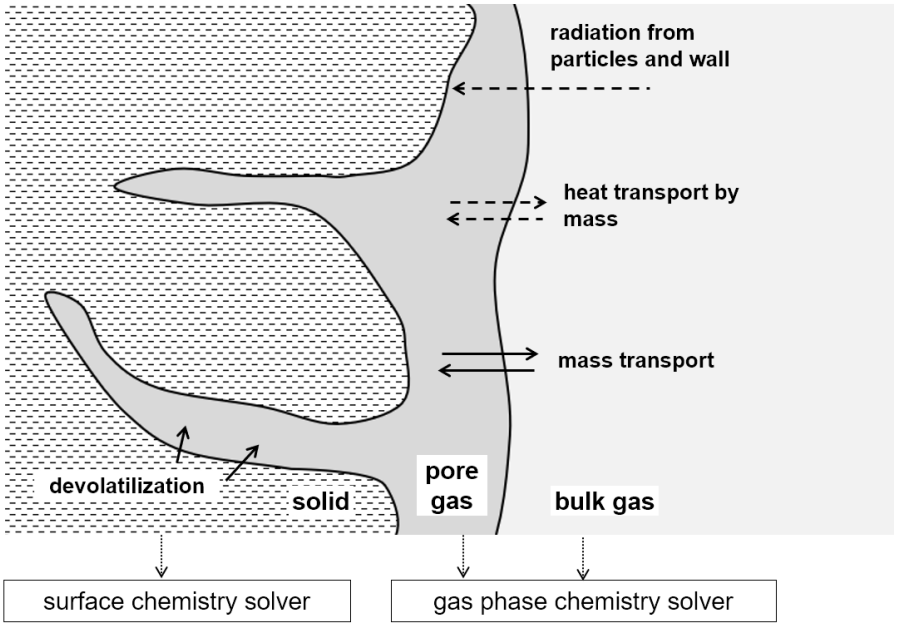

Figure 1: Schematic of the model.

1D and 2D setups chosen in this work. This setup choice is discussed later in section "Test cases". Between the reactors mass is exchanged in flow direction. This mass flow rate is predefined according to the given boundary conditions and includes the composition of solid, pore and bulk gas as well as the temperatures of all three phases. In case the reactor is connected to a gas outlet (top of the bed), only the bulk gas is transferred. In this work, the mass flow rate between the reactors is determined a priori and updated. The mass flow rate prediction based on the reactor outlet will be automated and addressed in future work.

Initially the solid and gas phases are defined separately and fed to an inlet reactor. The purpose of this inlet reactor is to mix the gas and solid phase and to create stochastic particles that are needed to feed the reactors in the network. For the mass transfer, at each time step, stochastic particles are chosen randomly and transferred to the next reactor and used to create a new stochastic particle until the mass of the transferred particle is consumed. In case a particle is not consumed completely, it is "remembered" and passed on to be transferred in the next time step. In this way, the inhomogenity created by stochastic mixing and heat transfer in the reactor is kept, as transferring the mean species composition

and temperatures would lead to an averaging and homogenization. The mass transfer to the next reactor produces new particles at each time step, so that the average particle number at the the end of the simulation is about 100 stochastic particles per reactor. 50 to 100 particles per reactor have been shown to mimic the distribution of physical quantities within gasification processes[52] and to reproduce good results for gas phase species and temperature in a reactor network compared to CFD simulations.[63] In this work, using 100 particles the results are found to be converged; a smaller number of particles lead to discretization errors, faster homogenization and a homogeneous reactor like behavior, a larger number of particles to a significant increase of simulation time without gain in accuracy of the results. The mixing time is set for all reactors and cases to 1 s. This results in one mixing realization per operator splitting loop and leads to low mixing, accounting for the low turbulent flow through the waste bed. For comparison, highly turbulent flows such as in an entrained flow gasifiers or internal combustion engine are in the order of magnitude of 0.001 to 0.05 s.[53]

The chemical model

The detailed reaction mechanism by Ranzi et al.[16] is used to predict the kinetics of biomass pyrolysis and devolatilization reactions, char reactivity, secondary gas-phase reactions and tar conversion. The scheme includes cellulose (CELL), hemicellulose (HCE) and lignin species with different H:C:O-ratios (LIG_C =$C_{15}H_{14}O_4$, LIG_H=$C_{22}H_{28}O_9$, LIG_O=$C_{20}H_{22}O_{10}$ with the indices indicating the dominant molecule) as surrogate components to represent woody biomass. Additionally, the ash and moisture content can be specified. The surrogate is defined based on the H:C:O-ratio of an ultimate composition analysis (UCA) using a mixing triangle in the C-H space of mixtures of CELL/HCE, LIG_C/LIG_H and LIG_C/LIG_O.[15,64] In this work, this methodology is adopted, but under the assumption that the hydrogen (H_2) fraction needs to be as close as possible to the experimental analysis to respect the lower heating value and hydrogen release. Therefore, the surrogate is optimized to match the hy-

drogen content of the UCA. Both the ash and water content are set to match the proximate composition analysis given in the references.[7,14,54] All applied surrogates are listed in Table 1. In the devolatilization model, beside the surrogate species and their intermediate active species, also some species trapped in the solid matrix or the condensed phase (metaplastics, G{CO}, G{CO_2}, G{COH_2}) are included.[15] Char conversion and drying are accounted for by Arrhenius type expressions given in Table 2. The high-molecular-weight species released to the gas phase are representative species. Cellulose releases levoglucosan ($C_6H_{10}O_5$) and hydroxyl-acetaldehyde ($C_2H_4O_2$). Hemicellulose releases xylan ($C_5H_8O_4$). Lignin species release phenol (C_6H_5OH) and phenoxy species, here represented by $C_9H_{10}O_2$, and $C_{11}H_{12}O_4$.[16] Their breakup and the decomposition to other smaller released gases (e.g. methane (CH_4), ethane (C_2H_4)) are described by detailed gas phase reactions. In total, the mechanism includes 18 species and 23 reactions for the solid and heterogeneous reaction description, and 130 species and 3093 reactions for the gas phase. For more details on the kinetic scheme the reader is referred to other studies.[15,16,65]

Table 1: UCA of the wood pellets from,[7,14,54] H:C:O ratio and composition of the surrogate. All data in (wt%).

	Case 1 Softwood	Case 1 Hardwood	Case 2	Case 3
UCA experiments				
C	48.6	49.5	48.8	53.5
H	6.0	6.0	6.9	5.9
O	43.0	44.3	43.5	40.6
HCO ratio surrogate				
C	52.1	53.3	52.4	57.3
H	6.2	6.2	6.2	6.3
O	41.7	40.5	41.4	36.5
Surrogate composition				
CELL	42.3	40.5	42.1	13.7
HCE	28.2	27.0	28.1	9.2
LIG_C	4.0	5.1	4.3	4.8
LIG_H	16.1	20.5	17.1	19.0
LIG_O	0.0	0.0	0.0	0.0
Water	7.2	6.4	8.3	52.9
Ash	2.1	0.4	0.1	0.4

In this work, the gas phase mechanism is subsequently reduced using the necessity analysis

Table 2: Trapped species (A), char conversion model (B) and drying (C) according to Ranzi et al.[16]

Type	Reaction	Pre-exponential factor A 1/s	Activation energy E_a KJ/mole
(A)	$G\{CO_2\} \rightarrow CO_2$	1.00E+05	100.4
(A)	$G\{CO\} \rightarrow CO$	1.00E+13	209.2
(A)	$G\{COH_2\} \rightarrow CO+H_2$	5.00E+11	272.0
(A)	$G\{H_2\} \rightarrow H_2$	1.00E+10	188.3
(B)	$Char+O_2 \rightarrow CO_2$	5.70E+15	159.8
(B)	$Char+H_2O \rightarrow CO+H_2$	7.90E+15	217.6
(B)	$2\ Char+O_2 \rightarrow 2CO$	2.85E+17	230.1
(C)	$H_2O(S) \rightarrow H_2O$	1.00E+13	168.5

and mechanism reduction tools within LOGEresearch v1.10.[53] Within the reduction process the speciation of the high-molecular-weight released species and ignition delay time (IDT) of single species as well of typical mixtures are controlled, as suggested in a previous work.[66] The reduction results in a gas phase model with 83 species and 1458 reactions. Any further reduction leads to significant changes in the speciation prediction of the larger molecules. This effect is also discussed in a previous study.[67] The reduced reaction scheme and its validation is given in the supplementary materials.

Test cases

Three test cases are chosen for the validation of the fuel bed model. The case setups are illustrated in Figure 2, while operating specifications and the solid fuel surrogate compositions are summarized in Table 3 and Table 1 respectively.

The first test case is targeted to validate the pyrolysis prediction approach and speciation under pyrolysis conditions. Dupont et al.[14] report experimental data obtained using a lab-scale entrained flow reactor operating at 1073 K and 1273 K. Nitrogen is fed with a flow rate of 16 l/min resulting in laminar flow conditions. Two types of wood pellets with various particle sizes have been investigated: a softwood mixture with a flow rate of 1 g/min and

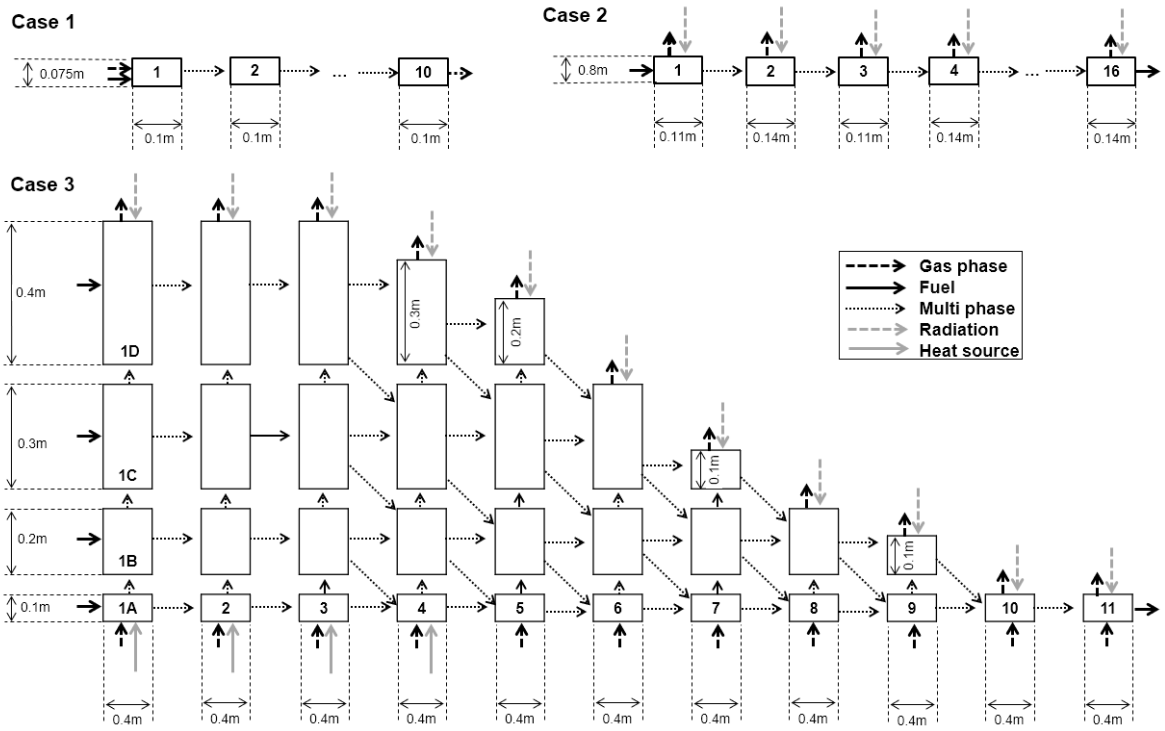

Figure 2: Reactor network for the different test cases.

a hardwood mixture with 0.5 g/min. The fuel specification as reported by Dupont et al.[14] and the corresponding surrogate used in this work are given in Table 1. The reactor is 1.0 m long with an inner diameter of 7.5 mm. The reactor network is discretized into 10 reactors. The EFR is iso-thermal between 0.30 and 0.95 m which is respected in the simulation by setting adiabatic temperature conditions. Nitrogen and fuel are fed in a co-flow configuration (Figure 2).

Table 3: Overview of the test cases and their model setups.

	Case 1	Case 2	Case 3
Reference	Dupont et al.[14]	Ahn and Jang[7]	Razmjoo et al.[54]
Type	EFR	Traveling grate	Traveling grate
Gas phase	N_2	air	air
Flow	co-flow	cross-flow	cross-flow
Ignition	-	from top	from grate

The second test case is a 16 step grate-fired wood pellet boiler. The prototype by Ahn

and Jang[7] is targeted to yield a combustion load of 230 kW at a fuel feed rate of 50 kg/h and an air supply of 547 Nm^3/h. The air is supplied from the bottom of the grates and is assumed to be evenly distributed over the fuel bed.The grate is 2 m long and 0.9 m wide. The computational domain of the combustion chamber is 2.5 m long (2 m grate and 0.5 m ash trap), 0.9 m wide and 1.6 m high at its maximum. The authors provided temperature measurements above the fuel bed for different loads, emissions in the flue gas, and performed also CFD simulations. In this work, the combustion loads of this prototype at 60%, 100% and 120% are reproduced by discretizing the 16 grates into 16 reactors in a row with alternating 110 mm and 140 mm length. Hereby, the intended turnover of the fuel at the grate steps can be represented by the mixing within the reactors. Air is fed to each reactor from the side and extracted at the top, while the fuel is feed to the first reactor and its product extracted at the last. The temperatures measured in the experiment are imposed as boundary conditions for the radiation onto the fuel bed. The predicted gas phase composition is in a second step used as boundary conditions of 2D CFD simulations using OpenFoam version 7.[68] The standard k-ε turbulence model,[69] the Eddy Dissipation Concept (EDC) in the version of Magnussen[70] together with the tabulation of dynamic adaptive chemistry (TDAC) model[71] and the P1 radiation model are applied. In the CFD, the reduced chemistry scheme by Li et al.[67] is used thanks to its small size of 32 species and 255 reactions and hence an affordable CPU time for large scale simulations is achieved. The size of the freeboard is adopted from the work of Ahn and Jang.[7] The CFD domain is discretized into a regular mesh with 30 000 cells each about 1 mm x 1 mm. The air is assumed to be equally distributed over the grate bars as indicated for the experiments,[7] which results in a velocity boundary condition of 0.725 m/s at full load conditions in 2D simulation. The boundary condition for turbulent kinetic energy is set to k=0.001 m^2/s^2 and its dissipation to $\epsilon = 0.1\ m^2/s^3$, in order to account for the low turbulence flow through the grate and fuel bed.[7]

The highlights of the third test case are the species and temperature measurements within

the fuel bed. Razmjoo et al.[54] report vertical temperature profiles and species profiles (O_2, CO, CO_2, CH_4 and NO) for the first grates. Measurements were taken in a 4 MW biomass-fired reciprocating grate boiler in which woody residues of a sawmill with a moisture level of 53% mass percent are converted. The grate is 5 m long and 1 m wide. The 5 m length are dived in a ramp of 0.6 m, followed by 11 grate bars with a length of 0.4 m each. Razmjoo et al.[54] report that the fuel bed is kept thick by purpose so that a high pressure drop leads to a more uniform flow which protects the grate during operation. As a consequence, the fuel bed is about 1 m at the upper part of the grate. Due to the thickness of the bed, the combustion of the biomass starts at the bottom of the fuel layer just on top of the grate, which has temperatures up to 1300 K.[54] To resolve also the vertical measurement, the bed is discretized into a matrix of 11 reactors along the grate. Further, to resolve the measurement locations over the fuel bed, reactors are stacked on top of each other. The dimensions are given in Figure 2. After the third grate the bed is assumed to collapse due to mass loss at the bottom of the bed and later also from the top. This is modelled as mass flow from the second row to the first and so on (diagonal arrows in Figure 2). The temperatures from the measurement at the grate are initialized as boundary conditions for the bottom layer to ignite the released gases, and for the top layer as a distribution analog to Case 2 representing the radiation from the freeboard.

Results and Discussion

Case 1

Figure 3 shows the validation of the reactor network and the reduced chemistry under pyrolysis conditions for softwood particles at two temperatures (1073 K and 1273 K). Other conditions such as particle size and composition, as well as air and fuel feed rates are the same in both experiments. Dupont et al.[14] highlight the trend in C_2H_4 and C_2H_2. At 1073 K, about three times more C_2H_4 than C_2H_2 is formed, while at 1273 K, more C_2H_2 than

C_2H_4 is formed, and the concentrations at reactor outlet are closer. The detailed chemical scheme (not shown) predicts first an increase in C_2H_4 and towards the end of the reactor a decrease.[14,15] The reactor network and reduced chemistry model can replicate this behavior. This is not directly seen in the experiments, but the predicted values are still close.

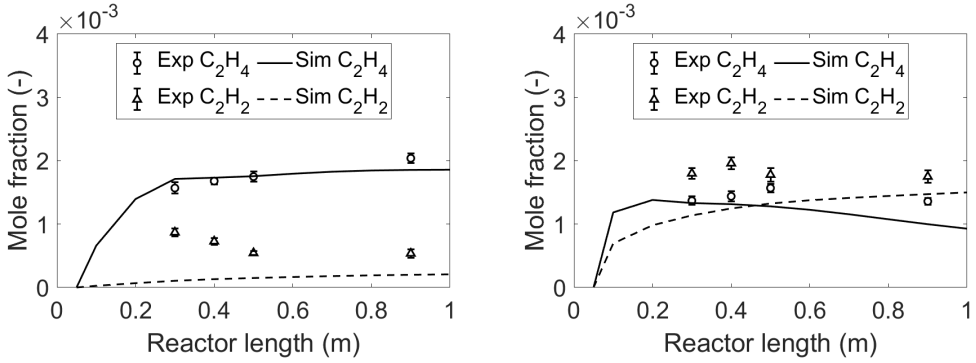

(a) 1073 K (b) 1273 K

Figure 3: Predicted gas release of softwood particles with a diameter of 0.45 mm at 1073 K and 1273 K. Experiments from Dupont et al.[14].

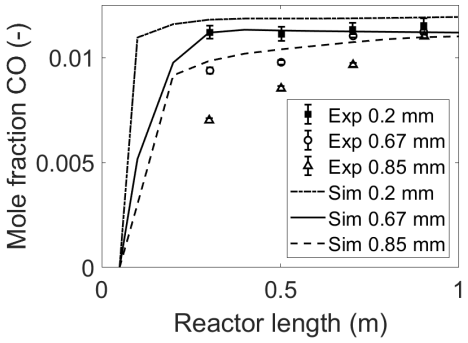

Figure 4: Predicted mole fraction CO as function of initial hardwood particles diameters at 1223 K. Experiments from Dupont et al.[14].

The predicted and measured CO molar fractions for hardwood particles with different sizes are shown in Figure 4. The particles' consumption is predicted faster within the reactor network than in the experiment. However, the absolute level and the trend in mole fractions of CO as function of the particle diameter are well reproduced at the reactor outlet.

The comparison to the experiments shows that using the reactor network and the reduced

chemistry scheme, speciation measurements under the tested pyrolysis conditions can be reproduced well and key pathways are maintained.

Case 2

In the following, the results of the fuel bed reactor network and the subsequent CFD simulations using the predicted released gas composition from the network as inlet conditions are discussed for different loads.

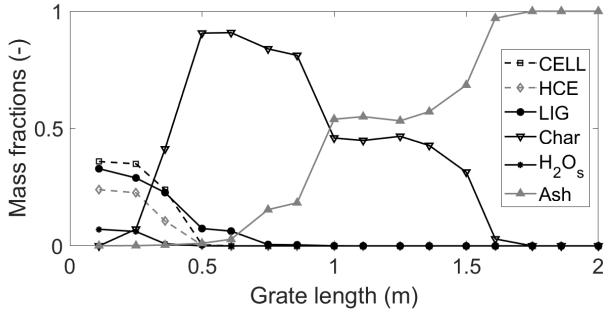

(a) Solid phase 100% load

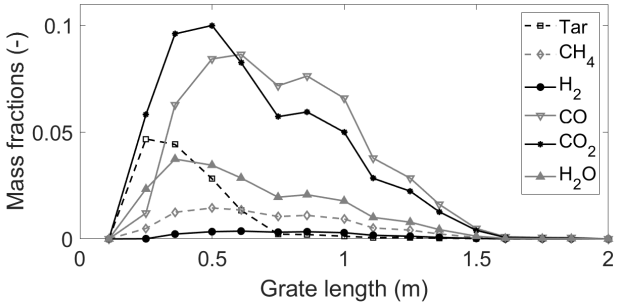

(b) Gas phase 100% load

Figure 5: Prediction of the compositions of solid and gas phase at 100% load conditions.

Figure 5(a) shows the predicted composition of the solid phase over the reactor length at 100% load. While the biomass is decomposed over the first grates, char is first formed and then burned, so that at grate 13 (1.75 m) only ashes remain. Ahn and Jang[7] stated that in the experiment almost no ash was found at the last three grate bars. By taking also the temperature measurement into account, they concluded that the combustion at

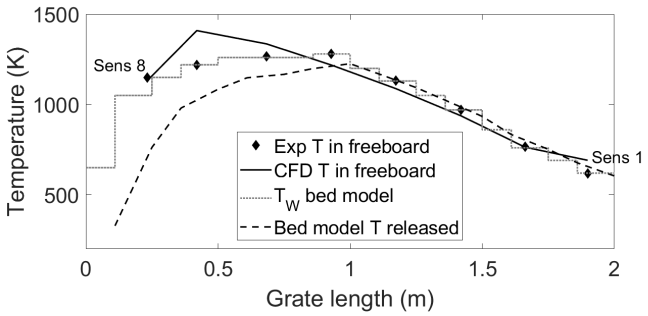

(a) Temperatures 100% load

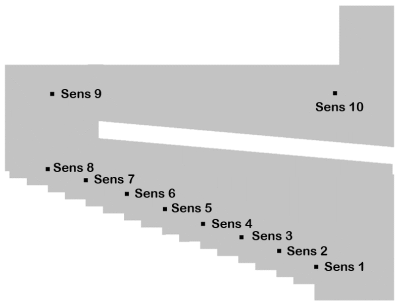

(b) Sensor positions

Figure 6: Prediction of gas and solid phase temperatures at 100% load conditions. Experiment and sensor positions from Ahn and Jang.[7]

100% load was completed at grate 12. The predicted solid composition goes well together with these observations since all combustible solid species are consumed and no more gases are released at the same grate (Figure 5(b)). The compositions of the solid and gas phase cannot be validated against experimental data as only temperature was measured, however the prediction is in line with literature: the lignin species known as the most durable parts of biomass with pyrolysis temperatures of 500 K to 770 K, remains longer than cellulose and hemicellulose.[72] Note that the figure shows the composition of the solid phase and not the absolute mass. In addition, different to the experiment, ash is not removed from the reactors, but carried with the solid mass flow. CO, CO_2 and small hydrocarbons are released over the whole fuel bed until grate 12, while tar species are released over the first grates only. The temperature prediction of the released gases by the bed model and the temperatures of the freeboard modelled in CFD are shown in Figure 6(a). The wall temperature included in

the figure shows how the measurement is used as input for the freeboard radiation onto the fuel bed. The temperature of the released gases in the first part (during tar release) is lower than the temperatures in the freeboard. Moving downwards the grate both temperature converge. Comparing the gas phase temperature prediction from the reactor network to the CFD temperature field as shown in Figure 11, this appears very plausible since the highest gas temperatures occurs during the oxidation in the freeboard and not directly above the fuel bed. A transition in the fuel bed is indicated by the drop in char concentration and released gases, as well as the convergence of the temperatures towards the outlet in Figure 6(a). At this point, most of the biomass is converted, char is no longer formed, but consumed over the reaming length of the grate.

In the following the fuel conversion is further analyzed and shown using only three representative grates that capture the devolatilization with maximum tar release at grate 2, the conditions at peak temperature and peak CO_2 release at grate 4, and the late burn out of the fuel at grate 10.

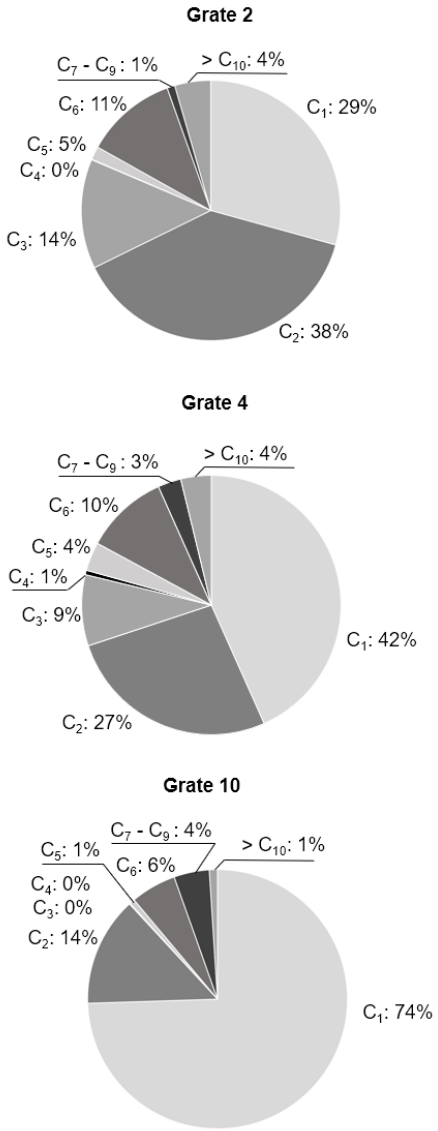

Figure 7: Composition by mass percentages of the released hydrocarbons of grate 2, grate 4 and grate 10 sorted by the amount of C-atoms.

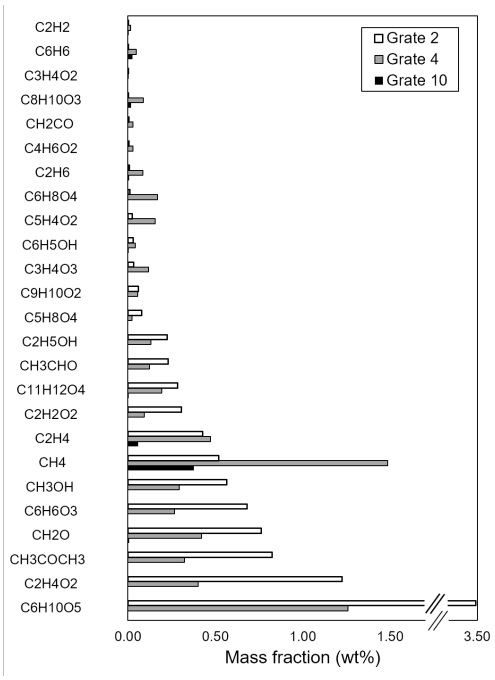

Figure 8: Released hydrocarbons (by mass) at the outlet to the freeboard at grate 2, grate 4 and grate 10. Hydrocarbons that have a mass percent >0.02 for one of the grate are selected.

Figure 7 and Figure 8 provide more details of the released gas phase composition. While Figure 7 shows the total amount of released hydrocarbons rated by their number of C-atoms, Figure 8 shows the most released hydrocarbons with a minimum concentration of 200 ppm at one of the reactors. At the first grate bar, larger molecules such as tar, C_2 and C_3 species are released. The species with the highest concentrations at grate bar 2 are $C_6H_{10}O_5$, $C_2H_4O_2$, CH_3COCH_3 and $C_6H_6O_3$ which are all released by the CELL model. This agrees with literature, since it is known that cellulose decompose faster and with less residue than hemicellulose and lignin.[72] At grate 2, also the hemicellulose and lignin decomposition has started, which can be followed up by their early decomposition products e.g. $C_{11}H_{12}O_4$, $C_9H_{10}O_2$ and $C_5H_8O_4$. While at grate 2 the most released species have minimum two C-atoms, species with only one C-atom are increasingly released downwards the bed, so that they form the biggest group. At grate 4, methane CH_4 has the highest mass concentration of all released hydrocarbons (Figure 8). At this grate, the devolatilization of the surrogate

species is still in progress, but the subsequent oxidation of the released tar is started, e.g. $C_8H_{10}O_3$ is build that is in the decomposition path way of $C_{11}H_{12}O_4$, and other species such as $C_6H_8O_4$ and $C_5H_4O_2$ are present. Biomass typically releases small C_2 hydrocarbons (C_2H_4 and C_2H_6) which are found at grate 4 in their highest concentration. At the end of the fuel bed, at grate 10 and with further progress in gas phase oxidation of tar species, only CH_4 and C_2H_4 are left in small amounts. During the combustion (here at grate 4 and grate 10) aromatic species and soot precursors are formed (C_6H_6 and C_2H_2).

Figure 9 gives more details about the inhomogenity of the stochastic reactors representing grate 2, grate 4 and grate 10. Shown are the PDFs in each of the reactors for gas phase temperature, available oxygen, released tar, CH_4 and CO. The PDFs of the gas temperature show that with increasing length of the fuel bed, the mean temperature is increasing for the selected reactors. Grate 2 has a wide temperature distribution from 300 K up to 1000 K. The maximum of the PDF is located at 850 K, but the distribution is comparable flat. Some particles are still relatively cold, while others release gases. At grate 4, the overall distribution is moved towards hotter temperatures between 450 K and 1200 K, but the flat structure of the PDF is retained. Stochastic particles represent very different temperature conditions, which leads to local differences in the devolatilization kinetics, conversion of solid fuel and released gases. At grate 10, close to the burn out of the solid fuel, the mean temperature is hotter, and more particles are located in the intervals close to the mean value. The temperature field is more homogeneous compared to the earlier grates. However, still a few particles and associated gas phases have quite low temperatures. The evolution of the gas phase temperature PDFs shows that the model approach indeed respects slow and non-uniform heating of the solid fuel entering the combustion chamber and the formation of hot and cold spots.

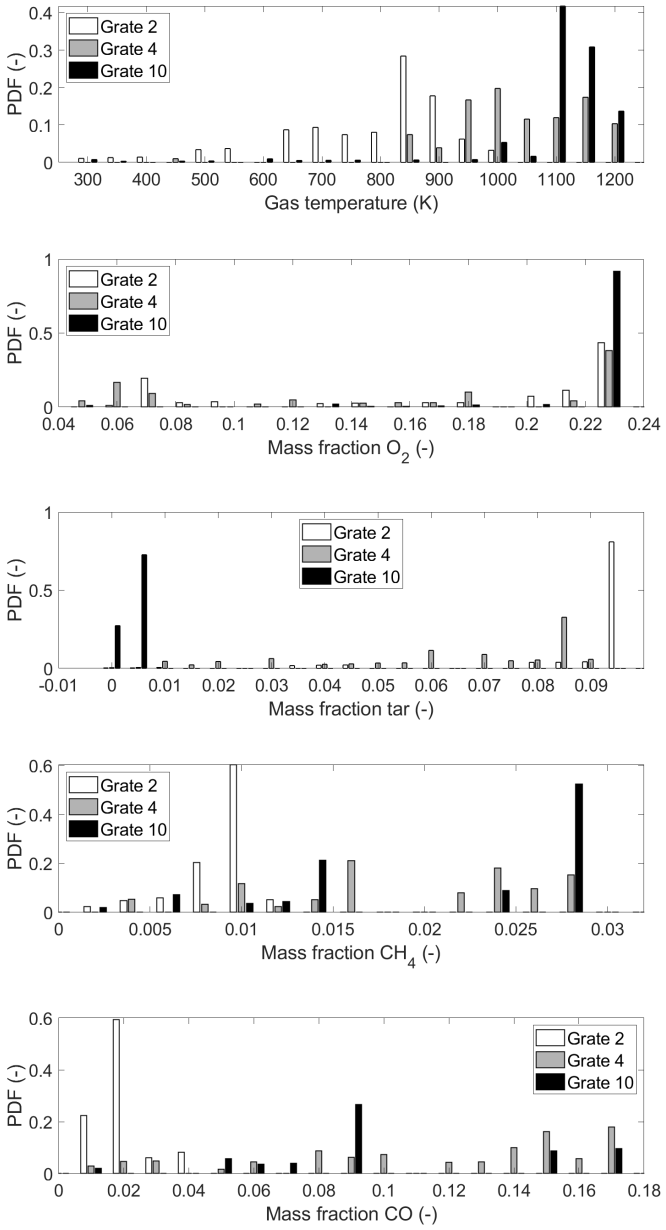

Figure 9: Probability density functions of the gas temperature and selected species mass fractions for three grate steps (grate 2, grate 4 and grate 10).

In a grate furnace, towards the fuel bed end, the temperature field is consistently more homogeneous since solid particles are smaller, cracked and more uniformly in size and composition, consisting mainly of char and ashes, and the fuel bed height is lower due to solid mass loss. In the reactor network model, as a result of mixing due to collapsing, here represented by merging of reactors, the bed is predicted overall to be more homogeneous. This effect is

more prominent with increasing bed length.

The distribution of O_2 has its maximum for all discussed grates at the composition corresponding to pure air. However, there is a number of stochastic particles with a lack of oxygen supply. For grate 2 and grate 4, a local maximum of very rich conditions is formed. This distribution can be interpreted to account for blocking of the grate and channel formation. This is due to that blocking of some grates result in very fuel-rich conditions, and subsequent channel formation to areas in the bed that are well supplied with oxygen. However, this effect needs further investigations to be verified. Just as the local temperature, the differences in available oxygen have a dominant impact on the local equivalence ratio and therefore on the released gases. The resulting distributions of released concentrations of tar, CH_4 and CO is evident of this impact. At grate 4, still some of the biomass surrogate components are present, while char is already formed. The variations in temperatures and available solid fuel and oxygen results in very flat distributed PDFs for tar species and other released gases, such as CH_4 and CO, and consequently to a very heterogeneously composed gas phase. At grate 2, this spread in gas phase composition is already evolving, but due to the early combustion progress, the majority of stochastic particles has a high concentration of tar and a low concentration of CO. The completion of the fuel conversion process is located at grate 10. No tar is released here, but the CH_4 and CO release are characterized by a wide and flat distribution. Overall, the temperature and species field that is found using the stochastic reactor network approach can be considered to be a realistic representation of a fuel bed undergoing thermal conversion and has an advantage over the use of homogeneous well-stirred reactors towards emissions and emission precursor prediction.

Based on the 100% load case, fuel and air flow rate are adjusted to represent 60% and 120% load and fed to the reactor network. The results of these operating conditions are presented in Figure 10(a). The tar release is for all loads comparable. This is due to the similar measured temperatures and accordingly set boundary conditions over the fist grates.

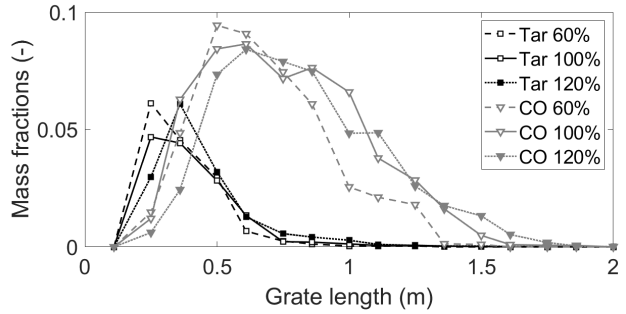

(a) Gas phase for different loads.

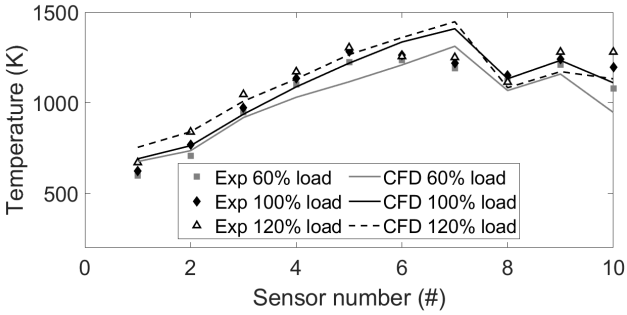

(b) Temperatures for different loads.

Figure 10: Gas phase prediction of the fuel bed model and temperature prediction of the freeboard using CFD for different loads. Location of the measurement sensors in Figure 6(b). Experiment from Ahn and Jang.[7]

Note that the composition of the gas phase is shown here, not the amount. However, the burn out of the char (here indicated by the CO release in Figure 10(a)) moves downwards the grate length with increasing load. Even though the fuel burn out is delayed for the high load of 120%, the wood pellets are still completely converted before reaching the end of the grate. Even though there are no validation data available, both observations indicate that the prediction align with general design practise of grate fired furnaces. The released gas composition and the gas phase temperature predicted using the reactor network are set as boundary conditions for the 2D CFD simulations to predict the temperature field in the freeboard. Figure 10(b) and Figure 11 show the freeboard temperature validations and 2D temperature predictions respectively. The location of the main flame and the general temperature field are both well reproduced compared to the CFD results in Ahn and Jang,[7]

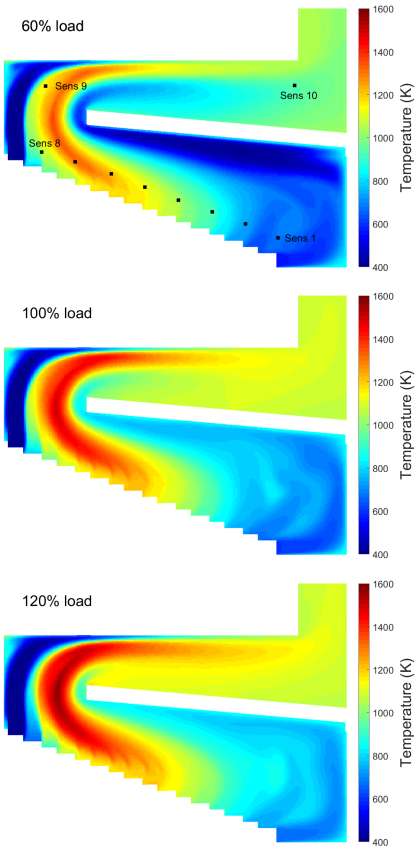

Figure 11: Temperature prediction of the freeboard for different loads. Black square show location of the measurement.[7]

as well as the measurements. This demonstrates that the presented approach can indeed serve for predicting boundary conditions for freeboard CFD simulations.

Case 3

The predicted vertical temperature gradient over the bed height compared to the measurement[54] are shown in Figure 12. The shown temperatures are the mean values at the stochastic reactor outlets. As discussed earlier, the temperatures are assigned to the bottom layer of the reactors to account for the ignition from the bottom of the fuel bed, and to the top layer to account for radiation from the freeboard. Both those heat sources can be recognized in the temperature profiles. The temperatures are somewhat over-predicted in the mid layer of the fuel bed, but the overall trends are kept well. This overestimation can be an effect

of the assigned gas mass flow that has to be assumed prior to the simulations. However, considering the uncertainty of the measurement locations that are estimated to be within 0.15 m of the specified positions,[54] the temperature profiles are considered as reasonably well predicted over the entire fuel bed height.

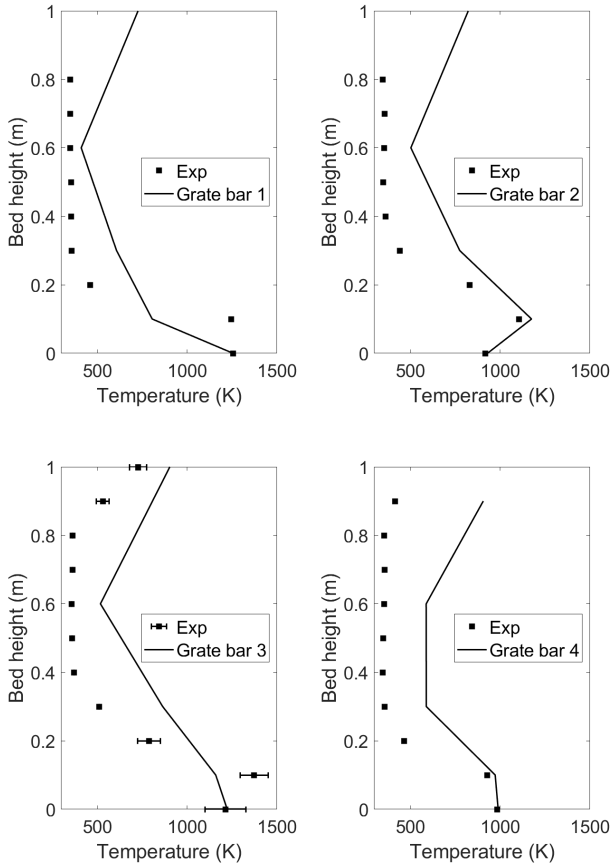

Figure 12: Temperature prediction over the fuel bed height. Experimental data from Razmjoo et al.[54]

For the second grate bar species measurements are available at 0.3 m and 0.6 m height. Comparisons to the measurements are shown in Figure 13 and Figure 14. The model predictions are related to dry measurement conditions. In the model, CO is formed close to the grate under high temperatures. Its concentration is reduced towards the top of the bed. At the height of 0.3 m, the concentration of CO is higher than in the gas released to the freeboard. Some of the CO gets oxidized to CO_2, but also in the upper region of the bed,

gases are released due to the temperature increase by radiation, which change the species ratios in the mixture. The heat supplied by radiation ignites the bed from top at about 2.7 m. This is indicated by the second peak in CO in Figure 14. CH_4 is produced close to the grate and in the hotter top layer. In the same region, tar species are released as shown in Figure 13. CO and CH_4 are well predicted over both bed height and length, as shown in Figure 14. CO_2 is under predicted for both locations, however its concentration increases with bed height which is seen to be the trend also in the experiments. The reasons for this can be a too slow conversion of CO to CO_2, or too little released CO_2 in the chemical model or as consequence of the formulated surrogate. This will be further investigated together with the model extensions to account for fuel NO formation in future work.

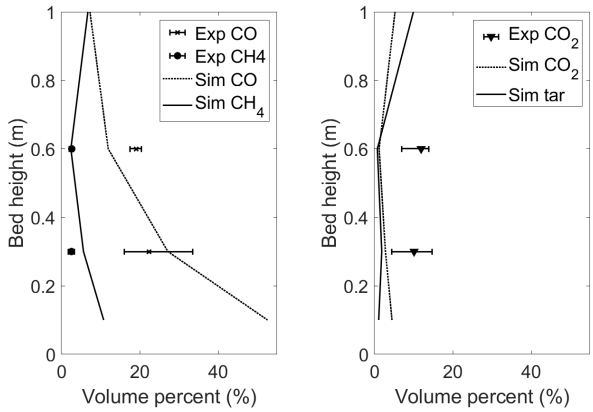

Figure 13: Species prediction over the fuel bed height at grate 2. Experimental data from Razmjoo et al.[54]

The overall drying and fuel decomposition in the fuel bed can be readily studied as presented in Figure 15 predicted by the reactor network. As shown in the upper diagram, drying takes place close to the grate where in the experiment combustion is observed, but also at the top layer due to the radiation from the freeboard. A wet layer between those zones remains. With grate length, this mid layer gets pushed towards the bottom of the fuel bed and heated up by radiation from the top, resulting in that after the seventh grate bar

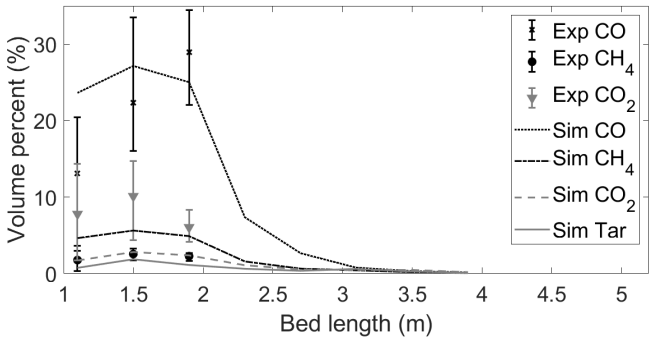

(a) Species at 0.3 m

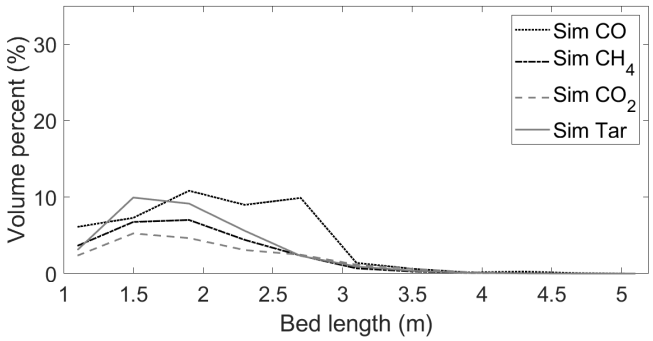

(b) Species at the top layer

Figure 14: Species prediction over the fuel bed length at 0.3 m bed height and of the reactors in the top layer of the network. Experimental data from Razmjoo et al.[54]

(3.5 m) the fuel is fully dried. The biomass is decomposed in a similar way as shown in the middle diagram. However, at the first grate bar, the fuel is dried only and not yet consumed. Starting from the reactors in the fourth column, the fuel gets mixed to the layer beneath (Figure 2). This results in an increase in biomass concentration in the bottom layer and a decrease in the top layer. From the lower diagram, one can see that char is formed mainly in the bottom layer of reactors, close to the grate to which high temperature sources are fed. This goes well with the findings from the experiment,[54] where the main conversion and the highest temperatures are found close to the grate. Additionally, some char is formed at the top layer, starting from reactor 3 (1.9 m), and at this point the radiation from the freeboard starts a second combustion spot. As discussed for the biomass, the mixing of mass from the layer above is visible in the char concentration starting from the fourth column. The fuel

and char is fully consumed at 4.3 m. This is also indicated by the released CO_2 and CO in Figure 14.

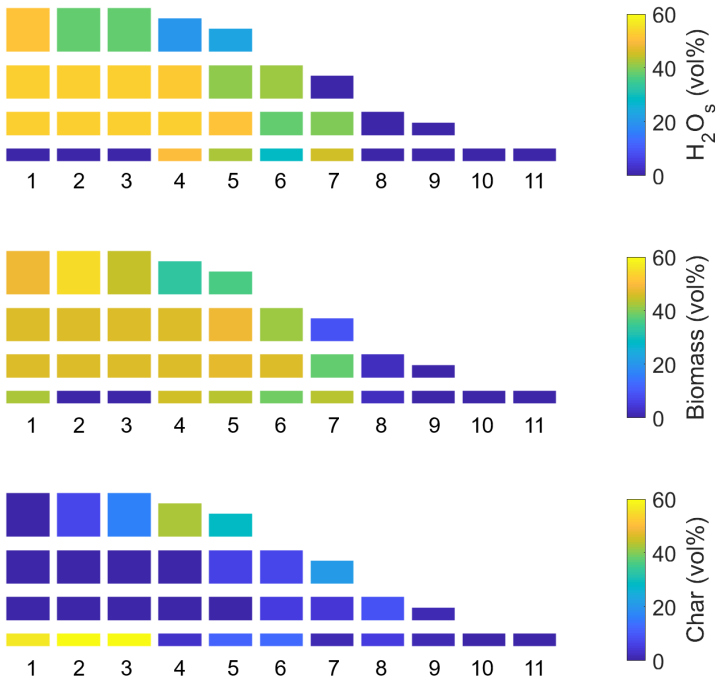

Figure 15: Predicted mean wt% of the solid phase in each of the reactors where H_2O_s is the moisture content of the solid fuel, and biomass includes all surrogate species as well as their early decomposition products species which are not further converted to char or metaplastics.

Summarizing, the reactor network can predict reasonable temperature and species profiles under these challenging conditions of wet fuel conversion. Further, the approach gives insight into the conditions within the fuel bed and of the released gas phase. The capabilities of the model allow its use in design and optimization tasks. Operating parameters of the fuel feed, such as mass flow and moisture content, and of the primary air, such as flow rate, temperature and amount of recirculated flue gas, can be modelled and analyzed to optimize the burn out of the fuel and to assess the risk of primary emission formation. Hereby, boundary conditions can be set based on educated guesses and do not necessarily come from an experiment. Reactor network models are well known to reduce CPU cost of otherwise costly CFD simulations down to minutes if single reactors are used. The computational

cost of a reactor network depend strongly and increase with the number of reactors, number of chemical species, and as in the presented model with the number of stochastic particles per reactor. In the applied discretization, using a total of 148 species and 3116 reactions, 340 minutes per reactor are needed to find converged results. This is higher than reported simulation time of other gasification processes using reactor network models, e.g by Du et al.[39] reporting 42 seconds simulation time for a network of 6 reactors, using only 7 species and 7 reactions for the modelling of air gasification of polyethylene, or by Li et al.[43] reporting a simulation time of 15 minutes for a network consisting of 7 reactors and using 7 species and 8 reactions to model an opposed coal multiburner gasifier. However, a direct comparison is challenging as the chosen model setups vary significantly with the chosen reaction mechanism size and the employment of homogeneous reactors rather than inhomogeneous. It is found that a considerable amount of the computational costs are caused by the mass transfer from one reactor to the other. Future work will address this limitation and a significant reduction in simulation time is expected.

Conclusion

A reactor network approach for the prediction of biomass conversion in grate fired furnaces using stochastic reactors is presented. The stochastic particles consist each of solid phase, pore and bulk gas and are a discrete realization of the joint probability density function of temperature and species composition. The approach is based on the use of detailed chemistry schemes, here reduced to a semi-detailed scheme, in order to study the released gases and emission precursors in detail. The model is tested using a pyrolysis case and two fuel beds in grate fired plants from literature that vary in complexity of the constructed reactor network and ignition type.

It has been shown that the developed reactor network can predict species and temperatures profiles over the fuel bed height and along the fuel bed length. Furthermore, the model

responds well towards load variations on all important physical parameters.

The use of stochastic reactors allow to model a non-uniform heating of the bed and distribution in primary air supply. Both heating and air distributions have an impact on the local species release and gas phase chemistry. The capacity to account for such effects are requirements for the analysis of emission formation that is strongly affected by local conditions.

Future work will update the solid particle treatment by a model that accounts for temperature gradients within the solid particle. Further, a reaction scheme and surrogate species that include fuel bonded nitrogen will be incorporated, and the fuel bed model will then be connected to a reactor network for the prediction of the freeboard combustion, so that also NO_x emissions can be analysed as this is one of the main concerns related to solid fuel conversion systems.

Acknowledgement

The authors acknowledge the financial support by the Knowledge-Building Project Grate-CFD (267957), which is funded by Statkraft Varme AS, EGE Oslo, Vattenfall AB, Hitachi Zosen Inova AG, Returkraft AS and LOGE AB, together with the Research Council of Norway through the ENERGIX program. UNINET Sigma2 and NTNU HPC Group provided high-performance computational resources.

Supporting Information Available

The following files are available free of charge.

- ReduceMechanism_mech.txt: reduced reaction mechanism file in standard format
- ReduceMechanism_therm.txt: thermal data file of the reduced reaction mechanism
- ReduceMechanism_tran.txt: transport data file of the reduced reaction mechanism

- Validation of the reduced reaction mechanism versus the detailed reaction scheme and experiments

References

(1) Klinghoffer, N.; Themelis, N.; Castaldi, M. *Waste to energy (WTE): An introduction*; Woodhead Publishing Limited, 2013.

(2) Glarborg, P.; Jensen, A.; Johnsson, J. Fuel nitrogen conversion in solid fuel fired systems. *Prog Energ Combust* **2003**, *29*, 89 – 113.

(3) Sefidari, H.; Razmjoo, N.; Strand, M. An experimental study of combustion and emissions of two types of woody biomass in a 12-MW reciprocating-grate boiler. *Fuel* **2014**, *135*, 120 – 129.

(4) Wiinikka, H.; Gebart, R.; Boman, C.; Boström, D.; Nordin, A.; Öhman, M. High-temperature aerosol formation in wood pellets flames: Spatially resolved measurements. *Combust Flame* **2006**, *147*, 278 – 293.

(5) Klason, T.; Bai, X. Computational study of the combustion process and NO formation in a small-scale wood pellet furnace. *Fuel* **2007**, *86*, 1465 – 1474.

(6) Ahn, J.; Jang, J. Combustion and heat transfer characteristics in a combustion chamber of a 13-step grate wood pellet firing boiler. *J Mech Sci Technol* **2018**, *32*, 1033 – 1040.

(7) Ahn, J.; Jang, J. H. Combustion characteristics of a 16 step grate-firing wood pellet boiler. *Renew Energ* **2018**, *129*, 678 – 685, 1st International Conference on Bioresource Technology for Bioenergy, Bioproducts Environmental Sustainability.

(8) Yang, Y. B.; Swithenbank, J. Mathematical modelling of particle mixing effect on the combustion of municipal solid wastes in a packed-bed furnace. *Waste Manage* **2008**, *28*, 1290 – 1300.

(9) Yin, C.; Rosendahl, L.; Kær, S. K.; Clausen, S.; Hvid, S. L.; Hille, T. Mathematical Modeling and Experimental Study of Biomass Combustion in a Thermal 108 MW Grate-Fired Boiler. *Energ Fuel* **2008**, *22*, 1380–1390.

(10) Advanced modelling and testing of a 13MWth waste wood-fired grate boiler with recycled flue gas. *Energ Convers Manage* **2016**, *125*, 230 – 241.

(11) Bermúdez, C. A.; Porteiro, J.; Varela, L. G.; Chapela, S.; Patiño, D. Three-dimensional CFD simulation of a large-scale grate-fired biomass furnace. *Fuel Process Technol* **2020**, *198*, 106219.

(12) Jell, S.; von Raven, R.; Spliethoff, H. Untersuchung der Stickoxidminderung in der thermischen Müllverwertung. *In Proceedings of 29. Deutscher Flammentag, German Section of the Combustion Institute* **2019**, Paper Number: IKV06.

(13) Frank, A.; Castaldi, M. CFD analysis of municipal solid waste combustion using detailed chemical kinetic modelling. *Waste Management and Research* **2014**, *32*, 745–754.

(14) Dupont, C.; Chen, L.; Cances, J.; Commandre, J.; Cuoci, A.; Pierucci, S.; Ranzi, E. Biomass pyrolysis: Kinetic modelling and experimental validation under high temperature and flash heating rate conditions. *J Anal Appl Pyrol* **2009**, *85*, 260 – 267.

(15) Ranzi, E.; Cuoci, A.; Faravelli, T.; Frassoldati, A.; Migliavacca, G.; Pierucci, S.; Sommariva, S. Chemical Kinetics of Biomass Pyrolysis. *Energ Fuel* **2008**, *22*, 4292–4300.

(16) Ranzi, E.; Pierucci, S.; Aliprandi, P.; Stringa, S. Comprehensive and Detailed Kinetic Model of a Traveling Grate Combustor of Biomass. *Energ Fuel* **2011**, *25*, 4195–4205.

(17) Anca-Couce, A.; Mehrabian-Bardar, R.; Scharler, R.; Obernberger, I. Kinetic scheme of biomass pyrolysis considering secondary charring reactions. *Energ Convers Manage* **2014**, *87*, 687–696.

(18) Anca-Couce, A. Reaction mechanisms and multi-scale modelling of lignocellulosic biomass pyrolysis. *Prog Energ Combust* **2016**, *53*, 41 – 79.

(19) Kinetic modeling of the thermal degradation and combustion of biomass. *Chem Eng Sci* **2014**, *110*, 2 – 12.

(20) Debiagi, P.; Pecchi, C.; Gentile, G.; Frassoldati, A.; Cuoci, A.; Faravelli, T.; Ranzi, E. Extractives Extend the Applicability of Multistep Kinetic Scheme of Biomass Pyrolysis. *Energ Fuel* **2015**, *29*, 6544–6555.

(21) Debiagi, P.; Gentile, G.; Cuoci, A.; Frassoldati, A.; Ranzi, E.; Faravelli, T. A predictive model of biochar formation and characterization. *J Anal Appl Pyrol* **2018**, *134*, 326 – 335.

(22) Hosseini Rahdar, M.; Nasiri, F.; Lee, B. A Review of Numerical Modeling and Experimental Analysis of Combustion in Moving Grate Biomass Combustors. *Energ Fuel* **2019**, *33*, 9367–9402.

(23) Collazo, J.; Porteiro, J.; Patiño, D.; Granada, E. Numerical modeling of the combustion of densified wood under fixed-bed conditions. *Fuel* **2012**, *93*, 149 – 159.

(24) Peters, B.; Schröder, E.; Bruch, C. Measurements and particle resolved modelling of the thermo- and fluid dynamics of a packed bed. *J Anal Appl Pyrol* **2003**, *70*, 211 – 231.

(25) Nasserzadeh, V.; Swithenbank, J.; Jones, B. Effect Of High Speed Secondary Air Jets On The Overall Performance Of A Large MSW Incinerator With A Vertical Shaft. *Combust Sci Technol* **1993**, *92*, 389–422.

(26) Costa, M.; Massarotti, N.; Indrizzi, V.; Rajh, B.; Yin, C.; Samec, N. Engineering bed models for solid fuel conversion process in grate-fired boilers. *Energy* **2014**, *77*, 244 – 253.

(27) Zadravec, T.; Yin, C.; Kokalj, F.; Samec, N.; Rajh, B. The impacts of different profiles of the grate inlet conditions on freeboard CFD in a waste wood-fired grate boiler. *Appl Energ* **2020**, *268*, 115055.

(28) Li, T.; Thunman, H.; Ström, H. A fast-solving particle model for thermochemical conversion of biomass. *Combust Flame* **2020**, *213*, 117 – 131.

(29) Mason, P.; Darvell, L.; Jones, J.; Pourkashanian, M.; Williams, A. Single particle flame-combustion studies on solid biomass fuels. *Fuel* **2015**, *151*, 21 – 30.

(30) Xu, Y.; Zhai, M.; Jin, S.; Zou, X.; Liu, S.; Dong, P. Numerical simulation of high-temperature fusion combustion characteristics for a single biomass particle. *Fuel Process Technol* **2019**, *183*, 27 – 34.

(31) Zhang, J.; Li, T.; Ström, H.; Løvås, T. Grid-independent Eulerian-Lagrangian approaches for simulations of solid fuel particle combustion. *Chem Eng J* **2020**, *387*, 123964.

(32) Yang, Y.; Goh, Y.; Zakaria, R.; Nasserzadeh, V.; Swithenbank, J. Mathematical modelling of MSW incineration on a travelling bed. *Waste Manage* **2002**, *22*, 369 – 380.

(33) Yang, Y.; Yamauchi, H.; Nasserzadeh, V.; Swithenbank, J. Effects of fuel devolatilisation on the combustion of wood chips and incineration of simulated municipal solid wastes in a packed bed. *Fuel* **2003**, *82*, 2205 – 2221.

(34) Mahmoudi, A. H.; Besseron, X.; Hoffmann, F.; Markovic, M.; Peters, B. Modeling of the biomass combustion on a forward acting grate using XDEM. *Chem Eng Sci* **2016**, *142*, 32 – 41.

(35) Peters, B.; Schröder, E.; Bruch, C.; Nussbaumer, T. Measurements and particle resolved modelling of heat-up and drying of a packed bed. *Biomass Bioenerg* **2002**, *23*, 291 – 306.

(36) Yang, Y.; Sharifi, V.; Swithenbank, J. Numerical Simulation of the Burning Characteristics of Thermally-Thick Biomass Fuels in Packed-Beds. *Process Saf Environ* **2005**, *83*, 549 – 558.

(37) Schulze, S.; Nikrityuk, P.; Compart, F.; Richter, A.; Meyer, B. Particle-resolved numerical study of char conversion processes in packed beds. *Fuel* **2017**, *207*, 655 – 662.

(38) Jourdan, N.; Neveux, T.; Potier, O.; Kanniche, M.; Wicks, J.; Nopens, I.; Rehman, U.; Le Moullec, Y. Compartmental Modelling in chemical engineering: A critical review. *Chem Eng Sci* **2019**, *210*, 115196.

(39) Du, Y.; Yang, Q.; Berrouk, A. S.; Yang, C.; Al Shoaibi, A. S. Equivalent Reactor Network Model for Simulating the Air Gasification of Polyethylene in a Conical Spouted Bed Gasifier. *Energ Fuel* **2014**, *28*, 6830–6840.

(40) *Rolls Royce Internal Report*; S.L. Bragg, 1953.

(41) Bauer, M.; Eigenberger, G. A concept for multi-scale modeling of bubble columns and loop reactors. *Chem Eng Sci* **1999**, *54*, 5109 – 5117.

(42) Lyra, S.; Cant, R. Analysis of high pressure premixed flames using Equivalent Reactor Networks for predicting NOx emissions. *Fuel* **2013**, *107*, 261 – 268.

(43) Li, C.; Dai, Z.; Sun, Z.; Wang, F. Modeling of an Opposed Multiburner Gasifier with a Reduced-Order Model. *Ind Eng Chem Res* **2013**, *52*, 5825–5834.

(44) Du, Y.; Sun, L.; Berrouk, A. S.; Zhang, C.; Chen, X.; Fang, D.; Ren, W. Novel Integrated Reactor-Regenerator Model for the Fluidized Catalytic Cracking Unit Based on an Equivalent Reactor Network. *Energ Fuel* **2019**, *33*, 7265–7275.

(45) Faravelli, T.; Bua, L.; Frassoldati, A.; Antifora, A.; Tognotti, L.; Ranzi, E. A new procedure for predicting NOx emissions from furnaces. *Comput Chem Eng* **2001**, *25*, 613 – 618.

(46) Shin, D.; Choi, S. The combustion of simulated waste particles in a fixed bed. *Combust Flame* **2000**, *121*, 167 – 180.

(47) Wurzenberger, J.; Wallner, S.; Raupenstrauch, H.; Khinast, J. Thermal conversion of biomass: Comprehensive reactor and particle modeling. *AIChE J* **2002**, *48*, 2398–2411.

(48) Yoon, H.; Wei, J.; Denn, M. A model for moving-bed coal gasification reactors. *AIChE J* **1978**, *24*, 885–903.

(49) Blasi, C. D. Dynamic behaviour of stratified downdraft gasifiers. *Chem Eng Sci* **2000**, *55*, 2931 – 2944.

(50) Chen, J.-Y. Stochastic Modeling of Partially Stirred Reactors. *Combust Sci Technol* **1997**, *122*, 63–94.

(51) Kraft, M. *Stochastic modeling of turbulent reacting flow in chemical engineering*; 1998.

(52) Weber, K.; Li, T.; Løvås, T.; Perlman, C.; Seidel, L.; Mauss, F. Stochastic reactor modeling of biomass pyrolysis and gasification. *J Anal Appl Pyrol* **2017**, *124*, 592 – 601.

(53) LOGEsoft v1.10, http://www.logesoft.com, 2018.

(54) Razmjoo, N.; Sefidari, H.; Strand, M. Measurements of temperature and gas composition within the burning bed of wet woody residues in a 4MW moving grate boiler. *Fuel Process Technol* **2016**, *152*, 438 – 445.

(55) Thunman, H.; Leckner, B. Ignition and propagation of a reaction front in cross-current bed combustion of wet biofuels. *Fuel* **2001**, *80*, 473 – 481.

(56) Thunman, H.; Leckner, B. Co-current and counter-current fixed bed combustion of biofuel—a comparison. *Fuel* **2003**, *82*, 275 – 283.

(57) Kraft, M.; Maigaard, P.; Mauss, F.; Christensen, M.; Johansson, B. Investigation of combustion emissions in a homogeneous charge compression injection engine: Measurements and a new computational model. *Prog Combust Inst* **2000**, *28*, 1195 – 1201.

(58) Tunér, M. Stochastic Reactor Models for Engine Simulations. Ph.D. thesis, LTH Lund University, 2008.

(59) Curl, R. Dispersed phase mixing: I. Theory and effects in simple reactors. *AIChE Journal* **1963**, *9*, 175–181.

(60) Pope, S. Small scales, many species and the manifold challenges of turbulent combustion. *Prog Combust Inst* **2013**, *34*, 1 – 31.

(61) Bhave, A.; Balthasar, M.; Kraft, M.; Mauss, F. Analysis of a natural gas fuelled homogeneous charge compression ignition engine with exhaust gas recirculation using a stochastic reactor model. *Int J Engine Res* **2004**, *5*, 93–104.

(62) Aslanjan, J.; Klauer, C.; Perlman, C.; Günther, V.; Mauss, F. Simulation of a Three-Way Catalyst Using Transient Single and Multi-Channel Models. *SAE Technical Paper* **2017**, Paper–No. 2017–01–0966.

(63) Nilsson, T.; Perlman, C.; Lehtiniemi, H.; Lörstad, D.; Möller, S.; Mauss, F. Gas Turbine Burner Reactor Network Construction and Application. *in 25th International Colloquium on the Dynamics of Explosions and Reactive Systems (ICDERS), 2-7 August, Leeds, UK* **2015**, 160.

(64) Cuoci, A.; Faravelli, T.; Frassoldati, A.; Granata, S.; Migliavacca, G.; Pierucci, S.; Ranzi, E.; Sommariva, S. A General Mathematical Model of Biomass Devolatilization. Note 2. Detailed Kinetics of Volatile Species. *in 30th Meeting on Combustion, Italian Section of the Combustion Institute* **2007**, 008.

(65) Grana, M. C. R.; Hemings, E. B.; Bozzano, G.; Dente, M.; Ranzi, E. Comprehensive Kinetic Modeling Study of Bio-oil Formation from Fast Pyrolysis of Biomass. *Energ Fuel* **2010**, *24*, 5727–5734.

(66) Seidel, L.; Netzer, C.; Hilbig, M.; Mauss, F.; Klauer, C.; Pasternak, M.; Matrisciano, A. Systematic Reduction of Detailed Chemical Reaction Mechanisms for Engine Applications. *J Gas Turbines Power* **2017**, *139*, 091701.

(67) Li, T.; Skreiberg, ; Løvås, T.; Glarborg, P. Skeletal mechanisms for prediction of NOx emission in solid fuel combustion. *Fuel* **2019**, *254*, 115569.

(68) Weller, H.; Tabor, G.; Jasak, H.; Fureby, C. A tensorial approach to computational continuum mechanics using object-oriented techniques. *Comput Phys* **1998**, *12*, 620–631.

(69) Launder, B.; Spalding, D. The numerical computation of turbulent flows. *Comput Method Appl M* **1974**, *3*, 269 – 289.

(70) Magnussen, B. THE EDDY DISSIPATION CONCEPT A BRIDGE BETWEEN SCIENCE AND TECHNOLOGY. *In ECCOMAS thematic conference on computational combustion* **2005**, 21–24.

(71) Contino, F.; Jeanmart, H.; Lucchini, T.; D'Errico, G. Coupling of in situ adaptive tabulation and dynamic adaptive chemistry: An effective method for solving combustion in engine simulations. *Prog Combust Inst* **2011**, *33*, 3057 – 3064.

(72) Zhao, C.; Jiang, E.; Chen, A. Volatile production from pyrolysis of cellulose, hemicellulose and lignin. *J Energy Inst* **2017**, *90*, 902 – 913.